High-Order Code Shift Keying for Ambient Backscatter Communications

Jixiang Chen, Quansheng Guan, *Senior Member, IEEE*, Yue Rong, *Senior Member, IEEE*, and Chuanlin Liu

***Abstract*— Ambient backscatter communication (AmBC) is a new advanced technology that utilizes ambient radio frequency signals to enable the communications of battery-free devices and has attracted much attention recently. Existing works develop the high-order modulation in signal domains including the time domain, the frequency domain and the space domain. However, the work in the code domain for AmBC remains missing. In this letter, we extend the high-order modulation to the code domain, i.e., high-order code shift keying (CSK). However, the detection that correlates the received signals with the candidate code cannot work due to the unknown source signals. To detect the active code index, the correlation energy detection (CED) is proposed in which the received signal energy instead of the amplitude is utilized. In this process, CED does not need the channel state information and source power knowledge. Simulation results show that the proposed CED can handle the complex source signal and achieve a desirable bit error rate (BER). The second-order CSK without the training sequences outperforms the on-off keying modulation with training sequences in terms of BER.**

***Index Terms*— Ambient backscatter communication, code shift keying, detection.**

I. Introduction

DUE to its low power consumption and low cost, ambient backscatter communication (AmBC) is regarded as a promising solution to a large scale deployment of future Internet of Things (IoT) networks [1]. In AmBC, there is no dedicated radio frequency (RF) source to be exploited for tag backscattering compared to conventional monostatic or bistatic backscatter communication. Instead, ambient signals like TV signals [2], FM signals [3] and Wi-Fi signals [4], [5] etc., can be used as source signals for the realization of AmBC.

Because of the low reflection efficiency and a large path loss, the strength of the backscattered signal is weak. Considering that tags are usually designed with a simple structure, most of the works on AmBC systems adopt binary modulation schemes, e.g., on-off keying (OOK) [2], [4], [6], [7], [8], [9], [10], [11], [12], [13]. The OOK modulation belongs to the binary amplitude shift keying (ASK), which means a low channel utilization for AmBC. If we increase the modulation order in the power (amplitude) domain, the difference in strengths of the backscattered signals will be small under the weak backscattered signal, which leads to poor detection performance. Thus, high-order modulation in the power domain is not practical for the tag. This necessitates exploring high-order modulation schemes in alternative signal domains.

Existing works have explored high-order modulation for AmBC. In the time domain [14], the authors propose the high order time shift keying to increase the channel utilization. Both coherent and non-coherent transmission schemes are studied. For the space domain [15], the authors employ multiple antennas at the tag and the reader to realize the space shift keying. The letter [16] explores the multiple frequency shift keying modulation in which multiple frequency bands and passband filters at the receiver are required to remove the direct link interference. In [17], the authors derive the optimal energy detector for the high order phase-shift keying for AmBC. However, research work in the code domain which is orthogonal to these domains is still scarce. The high order modulation in the code domain does not need additional hardware or required multiple frequency bands. It can be also integrated with other domains to achieve higher communication rates. For the sake of understanding, we make a comparison between the high order modulations over different signal domains in Table I.

This letter proposes the high-order code shift keying (CSK) modulation for AmBC for the first time, which increases the modulation order in the code domain to increase the channel utilization. With CSK, the ambient signal is backscattered using one of the codes chosen from the designed codebook. This code is referred to as the active code. CSK modulates its information by the position index of the active code within the codebook. In this sense, the channel utilization can be increased compared to binary modulation schemes.

To demodulate the CSK signal, the receiver needs to determine the index of the active code. The conventional operation for code-based detection is based on multiplication. That is, the received signal is multiplied with the candidate backscatter symbol vector chosen from the codebook [18], [19]. Then, the index of the maximum correlator's output is determined as the active code index. However, this operation cannot be applied directly to the AmBC system because the received signal contains the unknown source signal and all the correlation results will be indistinguishable. To address this problem, we propose correlation energy detection (CED), which exploits the energy vector of received signals to deal with the unknown source signals. After obtaining the energy vector, the receiver uses a candidate code to correlate with the energy vector. Consequently, the code with the maximum

Received 5 November 2024; revised 12 December 2024; accepted 4 January 2025. Date of publication 8 January 2025; date of current version 12 March 2025. This work was supported by the National Natural Science Foundation of China under Grants U23A20281 and 62341129, and the Science and Technology Planning Project of Guangdong Province of China under Grant 2023A0505050097. The associate editor coordinating the review of this letter and approving it for publication was H. Jung. *(Corresponding author: Quansheng Guan.)*

Jixiang Chen and Quansheng Guan are with the School of Electronic and Information Engineering, South China University of Technology, Guangzhou 510640, China (e-mail: eejxchen@mail.scut.edu.cn; eeqshguan@scut.edu.cn).

Yue Rong is with the School of Electrical Engineering, Computing, and Mathematical Sciences, Curtin University, Bentley, WA 6102, Australia (e-mail: y.rong@curtin.edu.au).

Chuanlin Liu is with Sichuan DOOV Intelligent Cloud Valley Company Ltd., Yibin 644000, China (e-mail: liu.zhuanlin@gmail.com).

Digital Object Identifier 10.1109/LCOMM.2025.3527463

TABLE I
ADVANTAGES AND LIMITATIONS OF HIGH ORDER MODULATIONS IN DIFFERENT SIGNAL DOMAINS

Signal domains	Advantages	Limitations
Code	No additional hardware or frequency bands; No need for training symbols and no detection threshold	Suffering from the direct-link interference
Time	Reducing the interference to the legacy users; No additional hardware or frequency bands; Less or no training symbols and no detection threshold	Suffering from the direct-link interference
Frequency	Removing the direct-link interference, and increasing the communication rate	Requiring frequency shift at the tag and multiple frequency bands and filters at the receiver
Space	Removing the direct-link interference, and increasing the communication rate	Requiring additional hardware at the tag and the reader
Power/Phase	Increasing the communication rate	Requiring multiple impedance; Requiring more training symbols to estimate parameters; Multiple detection thresholds for each source; Suffering from the direct-link interference

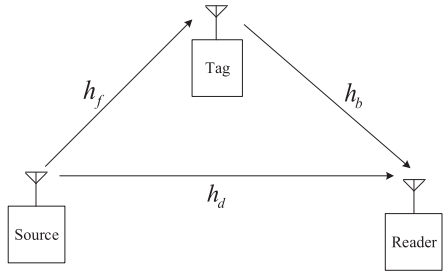

Fig. 1. System model of ambient backscatter communications. The ambient signal broadcasted by the source can be received by both the tag and the reader. The tag modulates the incident signal by varying its load impedance, and backscatters the modulated signal to the receiver.

correlation is considered as active one. Compared with existing methods such as OOK, the knowledge of the source power, channel state information and the detection threshold are not required at the receiver.

II. CSK FOR AMBC

In this section, we present the proposed CSK modulation for AmBC.

A. System Description

Consider an AmBC system consisting of a tag, a reader and an ambient RF source as shown in Fig. 1. Each of them is equipped with one antenna. The tag can harvest energy or transmit symbols by adjusting its impedance. The ambient source signal is harvested when the load impedance is matched, while the ambient source signal is reflected as the load impedance is mismatched. The reader receives both signals from the tag and the source simultaneously.

We denote the channel from the source to the reader as the direct channel h_d, the channel from the source to the tag as the forward channel h_f, and the channel from the tag to the reader as the backward channel h_b, respectively. We assume that the channels are block flat fading and independent from each other, as adopted by existing works [6], [7], [14], [15], [16].

B. Signal Model

With severe path loss and low backscatter efficiency, the backscattered signals are weak compared with the source signal. Thus, the duration of the backscattered symbol is usually extended to reduce communication errors. We assume that one CSK symbol includes N backscattered signals. Let us denote the n-th backscattered signal as $x(n)$, and the source signal as $s(n)$. Then the n-th received signal at the reader is

$$y(n) = h_d s(n) + h_b h_f \alpha x(n) s(n) + w(n), \tag{1}$$

where $n = 1, 2, \cdots N$, α is a coefficient representing the scattering efficiency and antenna gain, and $w(n)$ is the zero-mean additive white Gaussian noise (AWGN) with variance σ_w^2.

The tag adopts the CSK modulation to convey its information and the different code is chosen by different transmission bits. Assume that there are L codes in the codebook for CSK. In other words, the CSK codebook can be expressed as

$$\mathbf{X} = \{\mathbf{x}_1, \mathbf{x}_2, \cdots, \mathbf{x}_L\}, \tag{2}$$

where each $\mathbf{x}_l = [x_l(1), x_l(2), \cdots, x_l(N)], l = 1, 2, \cdots, L$ is a vector containing N backscattered signals. Then, the received signal can be rewritten in the vector form as

$$\mathbf{y} = \mathbf{s} \odot (h_d + \alpha h_b h_f \mathbf{x}) + \mathbf{w}, \tag{3}$$

where $\odot$ is Hadamard product [20]. The vector $\mathbf{y}$, $\mathbf{s}$ and $\mathbf{w}$ are $[y(1), y(2), \cdots, y(N)]$, $[s(1), s(2), \cdots, s(N)]$ and $[w(1), w(2), \cdots, w(N)]$ respectively. The vector $\mathbf{x}$ is chosen from $\{\mathbf{x}_1, \mathbf{x}_2, \cdots, \mathbf{x}_L\}$.

The codes in the codebook should be orthogonal to each other so that they can be distinguishable in the detection. There are some codebooks satisfying this requirement [21]. But considering the tag is usually produced with simple hardware,

a simple codebook is suitable for the tag. Thus, Hadamard matrix [22] is adopted in our CSK. CSK employs only two impedance for transmitting its information, which can be easily implemented at the tag. Let $\mathbf{C}_{2^p}$ be a Hadamard matrix of size 2^p. Then the partitioned matrix $\mathbf{C}_{2^{p+1}} = \begin{bmatrix} \mathbf{C}_{2^p} & \mathbf{C}_{2^p} \\ \mathbf{C}_{2^p} & -\mathbf{C}_{2^p} \end{bmatrix}$ is a Hadamard matrix of size 2^{p+1}. Note that $\mathbf{C}_1$=1. Thus, the size of Hadamard matrix can be infinite, and the orthogonality of this matrix is ensured, which means that there are no scalability limits in CSK. Part of the rows in Hadamard matrix is adopted as the codebook and the all-1 row is excluded. This is because we consider the source as a hidden tag and the all-1 row is its inherent code. Since other rows in Hadamard matrix are orthogonal to the all-1 row, the interference from source signals can be reduced. Due to the number of rows in Hadamard matrix is integer power of 2 and the all-1 vector cannot be used, we generate Hadamard matrix with $2L$ rows and choose only L rows as candidate codes to make up the codebook.

Each code in the codebook contains $M = 2L$ symbols. However, the number of backscattered signals N is usually much larger than M. To match the code with the transmission of backscattered signals, each symbol in a code is mapped to backscattered signals by copying itself $K = N/M$ times. Without loss of generality, we assume that the result of K is an integer.

The properties of CSK codes will be used in the sequel are

$$\mathbf{x}_l \mathbf{1}_{1\times N}^T = 0, \tag{4}$$

$$\mathbf{x}_l \mathbf{x}_l^T = N, \tag{5}$$

$$\mathbf{x}_l \mathbf{x}_{l'}^T = 0, l' \neq l, \tag{6}$$

$$\mathbf{x}_l \mathbf{s}^T \approx 0, \tag{7}$$

$$\mathbf{x}_l \mathbf{w}^T \approx 0, \tag{8}$$

where $\mathbf{1}_{1\times N}$ represents the all-1 row vector with a length N. The first three properties are intrinsic properties of Hadamard matrix. The last two properties are derived because the ambient source signal and noise are assumed to be zero mean. This assumption is reasonable since the source signal with the complex Gaussian (CG) distribution or phase-shift keying (PSK) or quadrature amplitude modulation (QAM) has zero mean. The AWGN noise is random and usually has zero mean leading to correctness of the last property in (8).

For ease of explanation, we take $L = 2$ and $N = 200$ as an example to illustrate our method. A $2L\times 2L$ Hadamard matrix $\mathbf{C}_4$ is given by

$$\mathbf{C}_4 = \begin{bmatrix} 1 & 1 & 1 & 1 \\ 1 & -1 & 1 & -1 \\ 1 & 1 & -1 & -1 \\ 1 & -1 & -1 & 1 \end{bmatrix}. \tag{9}$$

In this case, we can deduce that $M = 4$ and $K = 50$. We choose the second row and the third row for the codebook. Thus, the transmission vectors of backscattered symbols are $[\mathbf{1}_{1\times 50}, -\mathbf{1}_{1\times 50}, \mathbf{1}_{1\times 50}, -\mathbf{1}_{1\times 50}]$ for the second row and $[\mathbf{1}_{1\times 50}, \mathbf{1}_{1\times 50}, -\mathbf{1}_{1\times 50}, -\mathbf{1}_{1\times 50}]$ for the third row, where $-\mathbf{1}_{1\times K}$ represents the all--1 row vector with length K.

Since there are L codes for a backscattered symbol and only one code is chosen to backscatter signals, the tag can transmit $\log_2 L$ bits during one backscattered symbol. The number L usually takes an integer power of 2, so that a one-to-one mapping between input bits and active code indices can be realized.

III. Detection for CSK

In this section, we propose the CED detection for the CSK modulation. In order to mitigate the negative impact of source signals on the detection of the active code index, the received signals have a element-wise multiplication with its complex conjugate signals. The outcome of this operation is the energy vector of the received signal. Next, the candidate backscattered signal vector, i.e., one code from the CSK codebook, correlates with the received signal energy vector. In this process, the unknown source signals can be converted into a constant. Finally, the index of the maximum correlator's output is determined as the active code index.

In summary, the correlator's output in the CED detection can be conducted by calculating

$$\frac{|\mathbf{x}_t(\mathbf{y}\odot\mathbf{y}^*)^T|}{N}, \tag{10}$$

where the superscript $(\cdot)^*$ represents complex conjugate operation and $\mathbf{x}_t$ is chosen from $\{\mathbf{x}_1, \mathbf{x}_2, \cdots, \mathbf{x}_L\}$. Substituting (3) into (10), (10) becomes (11), as shown at the top of the next page. Since the $\mathbf{x}$ in (3) may be different from or the same as $\mathbf{x}_t$, we will discuss both two cases in the following. We use (12-i) and (13-i), $i = 1, 2, 3, 4, 5$, to refer to the i-th term in (12) and (13) respectively. For example, (12-1) is $\frac{\mathbf{x}_t}{N}\left[\mathbf{s}h_d \odot (\mathbf{s}\odot\alpha h_b h_f \mathbf{x}_t)^*\right]^T$. Note that $\mathbf{s}\mathbf{s}^H \approx NP_s$ when $s(n) \sim \mathcal{CN}(0, P_s)$, where $\mathcal{CN}(\mu, \sigma^2)$ denotes the complex Gaussian distribution with mean μ and variance σ^2, and P_s is the average transmission power of the source, $\mathbf{s}\mathbf{s}^H = NP_s$ when $s(n)$ is PSK modulated signal. For both types of source signals, $\mathbf{w}\mathbf{s}^H \approx 0$.

Case 1: $\mathbf{x} = \mathbf{x}_t$. Substituting $\mathbf{x} = \mathbf{x}_t$ into (11) and discarding terms unrelated to $\mathbf{x}_t$, (11) changes to (12), as shown at the top of the next page. The terms (12-1) and (12-2) equal to $P_s h_d(\alpha h_b h_f)^*$ and $P_s \alpha h_b h_f h_d^*$, respectively. The term (12-3) equals zero since it has three $\mathbf{x}_t$. Although (12-4) and (12-5) have two $\mathbf{x}_t$, they equal to zeros approximately since $\mathbf{w}\mathbf{s}^H \approx 0$. The final result in (12) is approximated as $2P_s\Re\left\{h_d(\alpha h_b h_f)^*\right\}$, where $\Re\{\cdot\}$ represents the real part of a complex number.

Case 2: $\mathbf{x} = \mathbf{x}_j, j \neq t$. Substituting $\mathbf{x} = \mathbf{x}_j$ into (11) and discarding terms unrelated to $\mathbf{x}_t$, (11) changes to (13), as shown at the top of the next page. The first two terms in (13) equal to zeros. This is because the element-wise multiplication between $\mathbf{x}_t$ and $\mathbf{x}_j$ has equal numbers of $+1$ and -1. The analysis to other terms in (13) is similar to that we mentioned in (12), and we omit here for brevity. The final result in (13) shown at the top of the next page is approximated as 0.

In summary, the final result in *Case 1* will be greater than that in *Case 2*. Thus, $\hat{\mathbf{x}}$ can be estimated by

$$\hat{\mathbf{x}} = \max_{\mathbf{x}_t} \frac{|\mathbf{x}_t(\mathbf{y}\odot\mathbf{y}^*)^T|}{N}. \tag{14}$$

Remark 1: Note that $2P_s\Re\left\{h_d(\alpha h_b h_f)^*\right\}$ and 0 are approximated values for (12) and (13), respectively.

$$\frac{\mathbf{x}_t}{N}\left[\begin{array}{c}[\mathbf{s}h_d\odot(\mathbf{s}h_d)^*+\mathbf{s}h_d\odot(\mathbf{s}\odot\alpha h_b h_f\mathbf{x})^*+\mathbf{s}\odot\alpha h_b h_f\mathbf{x}\odot(\mathbf{s}h_d)^*+\mathbf{s}\odot\alpha h_b h_f\mathbf{x}\odot(\mathbf{s}\odot\alpha h_b h_f\mathbf{x})^*]\\ +\mathbf{s}\odot h_d\odot\mathbf{w}^*+\mathbf{s}\odot\alpha h_b h_f\mathbf{x}\odot\mathbf{w}^*+[\mathbf{s}^*h_d^*\odot\mathbf{w}+\mathbf{s}^*\odot(\alpha h_b h_f\mathbf{x})^*\odot\mathbf{w}]+\mathbf{w}\odot\mathbf{w}^*\end{array}\right]^T \tag{11}$$

$$\mathbf{x}=\mathbf{x}_t,\Rightarrow\frac{\mathbf{x}_t}{N}\left[\begin{array}{c}\mathbf{s}h_d\odot(\mathbf{s}\odot\alpha h_b h_f\mathbf{x}_t)^*+\mathbf{s}\odot\alpha h_b h_f\mathbf{x}_t\odot(\mathbf{s}h_d)^*+\mathbf{s}\odot\alpha h_b h_f\mathbf{x}_t\odot(\mathbf{s}\odot\alpha h_b h_f\mathbf{x}_t)^*\\ +\mathbf{s}\odot\alpha h_b h_f\mathbf{x}_t\odot\mathbf{w}^*+\mathbf{s}^*\odot(\alpha h_b h_f\mathbf{x}_t)^*\odot\mathbf{w}\end{array}\right]^T \tag{12}$$

$$\mathbf{x}=\mathbf{x}_j,\Rightarrow\frac{\mathbf{x}_t}{N}\left[\begin{array}{c}[\mathbf{s}h_d\odot(\mathbf{s}\odot\alpha h_b h_f\mathbf{x}_j)^*+\mathbf{s}\odot\alpha h_b h_f\mathbf{x}_j\odot(\mathbf{s}h_d)^*+\mathbf{s}\odot\alpha h_b h_f\mathbf{x}_j\odot(\mathbf{s}\odot\alpha h_b h_f\mathbf{x}_j)^*]\\ +(\mathbf{s}\odot\alpha h_b h_f\mathbf{x}_j\odot\mathbf{w}^*)+[\mathbf{s}^*\odot(\alpha h_b h_f\mathbf{x}_j)^*\odot\mathbf{w}])\end{array}\right]^T \tag{13}$$

Such approximation is more accurate for source signals with constant envelop (such as PSK signals) than for random source signals (such as CG signals). For $s(n)\sim\mathcal{CN}(0,P_s)$, increasing P_s will also increase its variance, which leads to a bigger variation of (12) and (13) around $2P_s\Re\left\{h_d(\alpha h_b h_f)^*\right\}$ and 0, respectively.

Remark 2: Previous works on binary modulation or high-order modulation [6], [7], [14], [17] require to estimate channel state information related parameters to facilitate detection. Our proposed CSK and its detection method can function without exact channel state information or any estimated parameters. This advantage avoids sending multiple training symbols at the tag, increasing the transmission efficiency.

In addition, the detection thresholds in terms of different sources are different in the OOK symbol detection process [6]. In contrast, the proposed detection process is the same for any source signal that has zero mean. It means CSK can adapt to multiple types of sources and changes of the source without modifying its detection algorithm. Moreover, the knowledge of the source power is not required at the receiver since the active code index can be detected without calculating the detection threshold.

High-order modulation in the space and frequency domain needs additional hardware i.e., multiple antennas at the tag, or multiple frequency bands while CSK does not. Note that the signal domains including time, space and frequency are orthogonal to each other. Thus, the proposed CSK can be easily integrated with the other high-order modulation schemes to further enhance the transmission rate of AmBC. For example, CSK can be applied to the time slots of time domain modulation. In the active time slot, the tag uses active codes to backscatter. Then, the receiver can use CED to detect the indices of the active time slot and code simultaneously.

Remark 3: The analysis of complexity and energy efficiency for CSK is presented in the following. To make a fair comparison, we choose [6] and [7] where the system does not have additional hardware and frequency bands. The detection method used in [6] and [7] is the energy detection (ED) by calculating $\mathbf{y}^H\mathbf{y}/N$. Our CED detection is realized is by calculating (10). The traditional ED has N multiplications and $N-1$ additions while our CED has $2N$ multiplications and $N-1$ additions. However, our CSK does not need to send training sequences at the tag to estimate some parameters used in the symbol detection. As can be deduced from [6] and [7], the length of the training sequences is usually set as $8-12$ to achieve the best estimation accuracy. The computational complexity of the parameter estimation method in [6] and [7] is the same as ED. Define the length of the training symbols and data symbols as L_t and L_d respectively. Neglecting the additions in detections, we can roughly infer that CSK has a lower complexity if $L_d<L_t$. Thus, depending on the frame format, the total computational complexity of the method in [6] and [7] may be higher or lower than our method. Nevertheless, both CSK and OOK in [6] and [7] have low polynomial complexity during the detection, which is affordable to a plug-in receiver or even a passive receiver.

We consider the energy efficiency for a backscatter communication system as $R/(P_r+P_t)$ [23], [24], where R is the communication rate, P_t and P_r are the power consumption of the tag and the receiver circuit respectively. The power consumption of the receiver is mainly related to the detection complexity. The CSK tag has almost the same energy consumption compared to the OOK because it only needs to toggle its switch several times in one CSK symbol. However, the high-order CSK receiver can detect more bits than the OOK receiver in [6] and [7] and does not need to estimate parameters before the data detection.

IV. Simulation Results and Discussions

In this section, simulation results are presented to evaluate the performance of the CSK modulation for AmBC.

We set $h_d\sim\mathcal{CN}(0,10)$, $h_b,h_f\sim\mathcal{CN}(0,1)$. The coefficient α representing the scattering efficiency and antenna gain is 0.5. We use CG signals, i.e., $s(n)\sim\mathcal{CN}(0,P_s)$, and M-PSK signals as source signals. The source power P_s is assumed equal for both two sources and set to 1. Without loss of generality, the type of the M-PSK source is the 8PSK source. The SNR is defined as P_s/σ_w^2. Matlab is used to conduct the following simulations and more than 5000 channel realizations are made to get the average BER.

We first evaluate the impact of the SNR on BER. The value of N is set as 320. To provide a BER benchmark performance, we compare CSK with OOK proposed in [6]. The length of the training sequence used in [6] is set as 12. The proposed CSK with $L=2$ has almost the same BER performance as OOK for both two sources. Given that the CSK modulation is non-coherent while OOK in [6] is semi-coherent, CSK should have a worse BER. However, CSK achieves comparable performance to OOK by using $\{+1,-1\}$ in the Hadamard matrix. From Fig. 2, the BER decreases with the increase of SNR. As the SNR increases, the source power increases when the noise power is fixed. As shown in **Remark 1**, increasing P_s also increases the variance of (12) and (13) when the source signal is complex Gaussian distributed, which means the interference exists in the high-SNR level. The BER of 8PSK has no error floor and is much lower than that of CG source due to its constant envelope signal property. The symbol duration is the same for high-order CSK and OOK. Thus, the

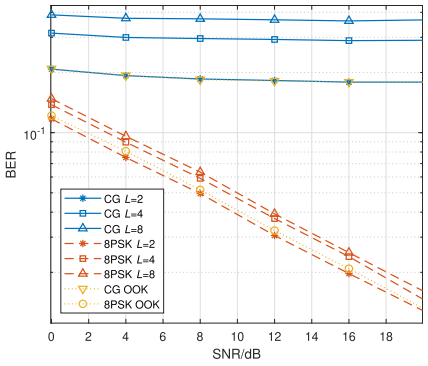

Fig. 2. BER versus SNR.

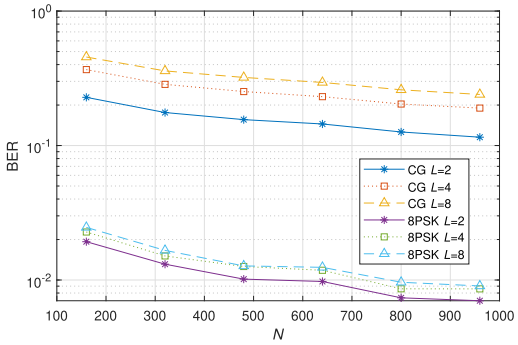

Fig. 3. BER versus N.

communication rate of CSK is $\log_2 L$ times of the OOK. That is, CSK has higher channel utilization than OOK for $L > 2$. For both sources, the increase of L leads to an increase in BERs. This means that a higher modulation order achieves a higher data rate at the cost of a high BER.

Next, the impact of the length of N on BER is studied. The SNR is set as 20 dB. It is obvious that a larger N results in a smaller BER for all cases, and there is no error floor in the large N region as shown in Fig. 3. To decrease the BER continuously, the tag can extend the duration of the backscattered symbol.

V. Conclusion

This letter has studied the CSK modulation and the CED detection for an ambient backscatter communication system. This CED detector can estimate the active code index by using the candidate code to correlate with the received signal energy vector. Thus, it is a non-coherent detector. We discussed the advantages of CSK over other modulation schemes. Simulation results show that high order CSK and its detection can be implemented for AmBC with satisfactory BER.

References

[1] T. Jiang et al., "Backscatter communication meets practical battery-free Internet of Things: A survey and outlook," *IEEE Commun. Surveys Tuts.*, vol. 25, no. 3, pp. 2021–2051, 3rd Quart., 2023.

[2] V. Liu, A. Parks, V. Talla, S. Gollakota, D. Wetherall, and J. R. Smith, "Ambient backscatter: Wireless communication out of thin air," in *Proc. ACM SIGCOMM*, Jun. 2013, pp. 39–50.

[3] A. Wang, V. Iyer, V. Talla, J. R. Smith, and S. Gollakota, "FM backscatter: Enabling connected cities and smart fabrics," in *Proc. 14th USENIX Symp. Netw. Syst. Design Implement. (NSDI)*, Mar. 2017, pp. 243–258.

[4] B. Kellogg, A. Parks, S. Gollakota, J. R. Smith, and D. Wetherall, "Wi-Fi backscatter: Internet connectivity for RF-powered devices," in *Proc. ACM Conf. SIGCOMM*, Aug. 2014, pp. 607–618.

[5] A. Abedi, F. Dehbashi, M. H. Mazaheri, O. Abari, and T. Brecht, "WiTAG: Seamless WiFi backscatter communication," in *Proc. Annu. Conf. ACM Special Interest Group Data Commun. Appl., Technol., Archit., Protocols Comput. Commun. (SIGCOMM)*, Jul. 2020, pp. 240–252.

[6] J. Qian, F. Gao, G. Wang, S. Jin, and H. Zhu, "Semi-coherent detection and performance analysis for ambient backscatter system," *IEEE Trans. Commun.*, vol. 65, no. 12, pp. 5266–5279, Dec. 2017.

[7] Q. Tao, C. Zhong, H. Lin, and Z. Zhang, "Symbol detection of ambient backscatter systems with Manchester coding," *IEEE Trans. Wireless Commun.*, vol. 17, no. 6, pp. 4028–4038, Jun. 2018.

[8] J. K. Devineni and H. S. Dhillon, "Non-coherent detection and bit error rate for an ambient backscatter link in time-selective fading," *IEEE Trans. Commun.*, vol. 69, no. 1, pp. 602–618, Jan. 2021.

[9] S. Guruacharya, X. Lu, and E. Hossain, "Optimal non-coherent detector for ambient backscatter communication system," *IEEE Trans. Veh. Technol.*, vol. 69, no. 12, pp. 16197–16201, Dec. 2020.

[10] Q. Tao, C. Zhong, X. Chen, H. Lin, and Z. Zhang, "Maximum-eigenvalue detector for multiple antenna ambient backscatter communication systems," *IEEE Trans. Veh. Technol.*, vol. 68, no. 12, pp. 12411–12415, Dec. 2019.

[11] T. Kim and W. Lee, "Exploiting residual channel for implicit Wi-Fi backscatter networks," in *Proc. IEEE Conf. Comput. Commun. (INFOCOM)*, Apr. 2018, pp. 1268–1276.

[12] G. Wang, F. Gao, R. Fan, and C. Tellambura, "Ambient backscatter communication systems: Detection and performance analysis," *IEEE Trans. Commun.*, vol. 64, no. 11, pp. 4836–4846, Nov. 2016.

[13] Y. Chen and W. Feng, "Novel signal detectors for ambient backscatter communications in Internet of Things applications," *IEEE Internet Things J.*, vol. 11, no. 3, pp. 5388–5400, Aug. 2024.

[14] J. Chen, H. Yu, Q. Guan, and W. Chen, "High-order time shift keying modulation and detection for ambient backscatter communications," in *Proc. IEEE/CIC Int. Conf. Commun. (ICCC Workshops)*, Dalian, China, Sep. 2023, pp. 1–6.

[15] A. H. Raghavendra, A. K. Kowshik, S. Gurugopinath, S. Muhaidat, and C. Tellambura, "Generalized space shift keying for ambient backscatter communication," *IEEE Trans. Commun.*, vol. 70, no. 8, pp. 5018–5029, Aug. 2022.

[16] Q. Tao, C. Zhong, K. Huang, X. Chen, and Z. Zhang, "Ambient backscatter communication systems with MFSK modulation," *IEEE Trans. Wireless Commun.*, vol. 18, no. 5, pp. 2553–2564, May 2019.

[17] J. Qian, A. N. Parks, J. R. Smith, F. Gao, and S. Jin, "IoT communications with M -PSK modulated ambient backscatter: Algorithm, analysis, and implementation," *IEEE Internet Things J.*, vol. 6, no. 1, pp. 844–855, Feb. 2019.

[18] G. Kaddoum, Y. Nijsure, and T. Hung, "Generalized code index modulation technique for high-data-rate communication systems," *IEEE Trans. Veh. Technol.*, vol. 65, no. 9, pp. 7000–7009, Sep. 2016.

[19] G. Kaddoum, M. F. A. Ahmed, and Y. Nijsure, "Code index modulation: A high data rate and energy efficient communication system," *IEEE Commun. Lett.*, vol. 19, no. 2, pp. 175–178, Feb. 2015.

[20] R. A. Horn, "The Hadamard product," in *Proc. Symposia Appl. Math.*, 1990, pp. 87–169.

[21] F. Rezaei, D. Galappaththige, C. Tellambura, and A. Maaref, "Time-spread pilot-based channel estimation for backscatter networks," *IEEE Trans. Commun.*, vol. 72, no. 1, pp. 434–449, Jan. 2024.

[22] K. J. Horadam, *Hadamard Matrices and Their Applications*. Princeton, NJ, USA: Princeton Univ. Press, 2007.

[23] Y. Ye, L. Shi, R. Qingyang Hu, and G. Lu, "Energy-efficient resource allocation for wirelessly powered backscatter communications," *IEEE Commun. Lett.*, vol. 23, no. 8, pp. 1418–1422, Aug. 2019.

[24] Y. Xu, B. Gu, and D. Li, "Robust energy-efficient optimization for secure wireless-powered backscatter communications with a non-linear EH model," *IEEE Commun. Lett.*, vol. 25, no. 10, pp. 3209–3213, Oct. 2021.